

# Cardiac Mesh Reconstruction from Sparse, Heterogeneous Contours

Benjamin Villard<sup>1</sup>(✉), Valentina Carapella<sup>2</sup>, Rina Ariga<sup>3</sup>, Vicente Grau<sup>1</sup>, and Ernesto Zacur<sup>1</sup>

<sup>1</sup> Institute of Biomedical Engineering, University of Oxford, Oxford, UK  
benjamin.villard@eng.ox.ac.uk

<sup>2</sup> Simula Research Laboratory, Bærum, Norway

<sup>3</sup> Division of Cardiovascular Medicine, Radcliffe Department of Medicine, University of Oxford Centre for Clinical Magnetic Resonance Research, University of Oxford, Oxford, UK

**Abstract.** We introduce a tool to reconstruct a geometrical surface mesh from sparse, heterogeneous, non coincidental contours and show its application to cardiac data. In recent years much research has looked at creating personalised 3D anatomical models of the heart. These models usually incorporate a geometrical reconstruction of the anatomy in order to understand better cardiovascular functions as well as predict different processes after a clinical event. The ability to accurately reconstruct heart anatomy from MRI in three dimensions commonly comes with fundamental challenges, notably the trade off between data fitting and regularization. Most current techniques requires data to be either parallel, or coincident, and bias the final result due to prior shape models or smoothing terms. Our approach uses a composition of smooth approximations towards the maximization of the data fitting. Assessment of our method was performed on synthetic data obtained from a mean cardiac shape model as well as on clinical data belonging to one normal subject and one affected by hypertrophic cardiomyopathy. Our method is both used on epicardial and endocardial left ventricle surfaces, but as well as on the right ventricle.

**Keywords:** Computational geometry · Mesh reconstruction · Cardiac modelling

## 1 Introduction

In recent years much research has looked at creating personalised 3D anatomical models of the heart [1–3]. These models usually incorporate a geometrical reconstruction of the anatomy in order to understand better cardiovascular functions as well as predict different processes after a clinical event. Besides being fundamental to shape analysis, they are the prerequisite to finite element analysis [4]. The ability to accurately reconstruct heart anatomy from magnetic resonance

imaging (MRI) in three dimensions commonly comes with fundamental challenges, notably the trade off between data fitting and regularization. Most works in the literature tend to over regularize, or bias the data fitting process towards a smooth result [5,6]. Other methods work based on templates or shape prior which are usually learned on normal patient anatomies, and tend to fail when presented with pathological data, or any data outside the learned model [7]. Our approach differs in this, as it minimizes the use of a regularization term while maximizes the data fitting. In this paper we discuss a process to reconstruct a geometrical 3D surface mesh from a set of contours available from manual delineations as well as from automatic segmentations. Cardiac contours are typically composed from a stack of short axes (SAX) ranging from 8–12 slices, and a couple long axes (LAX). As such the input data is quite sparse for conventional mesh reconstruction processes such as isosurfacing [8]. In manual contouring, clinicians are seldom able to account for the 3D environment which can lead to spatial discrepancies between long axes and short axes contours. For example, in LAX, papillary muscles can be hard to differentiate from myocardium which can result in their segmentation, in spite of their exclusion in SAX. Furthermore due to the image acquisition occurring at different breath hold, as well as any patient movement inside the scanner, the contours might be misaligned. This would further increase their discrepancies and extra steps might be needed to correct for this alignment [9]. This post-acquisition correction of the pose of the images can lead to loosing the parallelism in the SAX stack. Furthermore, due to the delineations not being able to grasp perfectly the overall shape of the heart, contour to contour distances cannot be minimized to obtain perfect coincidence and therefore spatial 3D consistency [9]. Finally, since many cardiomyopathies are localized in the left ventricle (LV), many previous efforts were focused on methodologies specifically designed or tuned for the LV. The main contributions of this work are:

- Use of our method on non parallel, sparse, heterogeneous contours
- Ability to deal with non coincidental contours
- Use of our technique on the right ventricle as well as the left ventricle.

## 1.1 State of the Art

Whilst simple heart models can be used for mechanical studies, patient-specific meshes require more complex anatomical models [10]. These models are characterized though 3D meshes, on which shape analysis or finite element methods (FEM) can be performed. From a set of contours or delineated curves, a surface mesh can be rendered and act as an input to generate a volumetric mesh. Depending on the complexity of the mesh needed, many parameters need to be taken into account; notably if the visual appearance of the mesh needs to be smooth [2,10]. In [2], the surface mesh is constructed by optimising over the topology, using a level-sets approach, and having the genus as a control parameter. Whilst this approach allows control over the topology, it can fail for sparse data. In order for the resulting mesh to represent the most accurate anatomical

representation, an image volume is necessary. In order to obtain uniformly distributed contour points, the authors in [11, 12], first fit a cubic periodic B-spline curve to the contours allowing them to uniformly sample candidate points. The disadvantages of this approach is that it relies on the the number of control points selected which in turn smooths the overall mesh. This is similar to [6], which can cause for the resulting mesh to be highly convoluted when dealing with pathological data. The method in [13] is closest to our own, as it tries to maximize the data fitting, whilst smoothing the interpolated part of the mesh.

## 2 Materials and Methods

### 2.1 Data

Both synthetic and clinical datasets were used. Synthetic contours were created from an average MRI mesh obtained from [14, 15] and are available online<sup>1</sup>. Using that mean shape, contours where synthesized by slicing the mesh at various spatial positions. Parallel and non parallel contours were produced and small random translations and rotations applied to the contours. We treated the initial mean shape mesh as ground-truth and compared our results against it. Clinical contours belonging to one normal subject and one affected by hypertrophic cardiomyopathy (HCM), were also used, which were delineated by experts on cine images at end-diastole.

### 2.2 Initial Mesh

Let  $\{C_j\}$  be a set of contours, each lying on a plane with normal  $n_j$ , where  $j$  is the contour index. The normals are clustered and the mean normal of the cluster group containing the most frequent orientation of the planes is calculated. The transformation matrix to align it with the  $Z$  axis is determined and is then applied to  $\{C_j\}$  such that the contours are in a common frame of reference aligned with respect to the  $Z$  axis. The contours with normals belonging to the cluster with the most frequent plane orientations (which are expected to be the ones in SAX view) are then sorted from the most apical to the most basal (see Fig. 1(a)). Two extra points are added to  $\{C_j\}$  providing an upper and lower lid, to fully enclose the initial mesh. We then proceed to create a rough initialization of the mesh by constructing a *tubular* surface going through the contours. For each of the contours, distribute  $K$  equally spaced contour points. A ruled surface approach is then used to obtain an initial mesh, where the initial triangle making up the mesh are composed of the set  $\{(C_j(i), C_j(i+1), C_{j+1}(i)), (C_{j+1}(i), C_{j+1}(i+1), C_j(i+1))\}$ , with  $i$  being the point index of the contours after resampling (see Fig. 1(b)). Depending on the availability of the LAX information, the algorithm initializes the upper mesh point as the mean position of the topmost contour points lying on the plane that contains such point. Analogously, the lower bound mesh point is initialized from the lowest contour points in that plane.

---

<sup>1</sup> <http://wp.doc.ic.ac.uk/wbai/data/>.

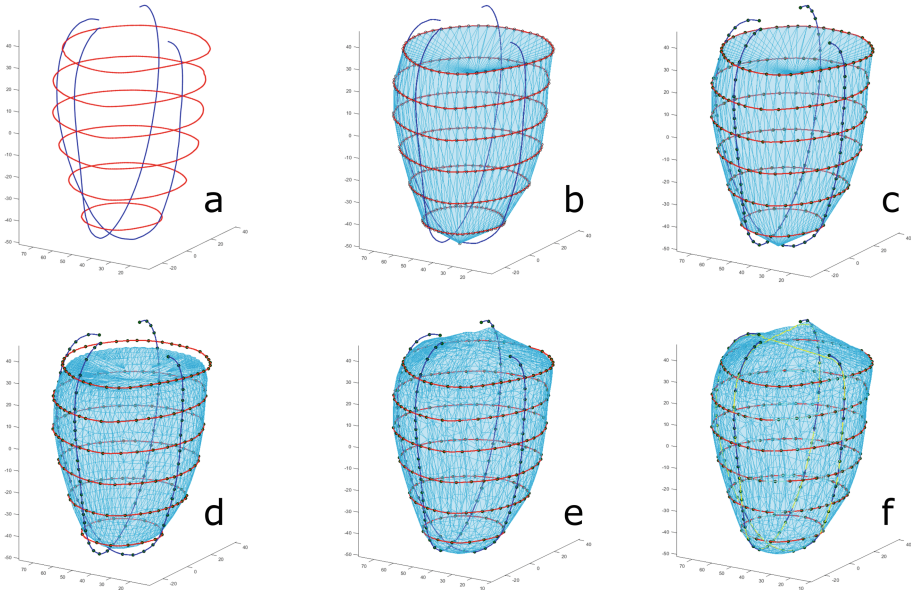


**Fig. 1.** Overall pipeline for generating a surface mesh from contours. (a) The input contours (red represents the automatically selected cluster group around the mean normal), (b) *Tubular* initial mesh, (c–e) different iterations of the process after deforming, subdividing and decimating the mesh, (f) final mesh. (Color figure online)

### 2.3 Mesh Deformation

Since the initial selected points make up the mesh, another set of contour points will be selected as the data fitting terms, and will act as attractors for the mesh.  $N$  number of points are sampled, where  $N \gg K$ , using farthest point sampling, allowing for a representation of the global spatial distribution of the contour points. The farthest point sampling method [16] ensures that no contour is sampled more densely than any others, and enforces an almost uniform global distribution of  $\{C_j\}$ . At this point, the initial mesh  $\mathcal{M}$ , the contours, and the attractors are all scaled to a common reference frame that is irrespective of the units of the provided contours. Once all the preprocessing is achieved, a deformation field is computed by taking the closest point from each of the attractor points to  $\mathcal{M}$ , and a dense force field is computed by using approximating thin plate splines [17, 18]. The mesh is then deformed by using the *inverse* of the force field. Let  $\{P_i\}$  be the set of closest points to  $\{Q_i\}$  lying on the surface  $\mathcal{M}$ . Let be  $F : \mathbb{R}^3 \Rightarrow \mathbb{R}^3$  such that:

$$\mathcal{M} = \min \lambda \sum_{i=1}^N (\|F(P_i) - (Q_i)\|)^2 + J_m^d(F) \quad (1)$$

where  $F$  is the mapping function, and  $J$  is the thin plate spline functional using derivatives of order  $m$ , and  $d$  the image dimensions, as defined in [17, 18]. We

perform this deformation iteratively, resulting in a composition of several smooth approximations of  $\mathcal{M}$  towards the contours. Once the mesh has been deformed, the mesh undergoes subdivision and quadratic decimation. By subdividing the mesh we increase its resolution allowing for a more appropriate reconstruction of the mesh. However, as this process can lead to extremely high amounts of triangles, the mesh is therefore decimated, which allows for some control over the amount of triangles while preserving its geometric characteristics [19]. Finally, the resulting mesh is smoothed, using Laplacian smoothing. The latter steps of subdivision, decimation and smoothing occurs every  $S$  iterations. We chose  $S$  empirically, to be 20. The overall pipeline can be seen in Fig. 1. The overall process starting from the farthest point sampling is repeated for a set number of iterations, or until some stopping criterion is achieved, such the contours-to-mesh distance falls below a chosen threshold.

### 3 Results

#### 3.1 Synthetic Data

**Short Axis Contours.** In order to assess our algorithm, we performed a series of experiments. In a first instance we applied our method to a set of parallel SAX contours and observed our technique’s ability to recover the ground truth mesh. We also assessed the effect the amount of SAX had on the quality of the mesh by increasing the amount of SAX contours provided initially from 2 to 15, between the base and the apex. Our validation consisted of calculating the distances between vertices of our generated mesh to the ground truth mesh (mean shape of the statistical model) and can be seen in Fig. 2.

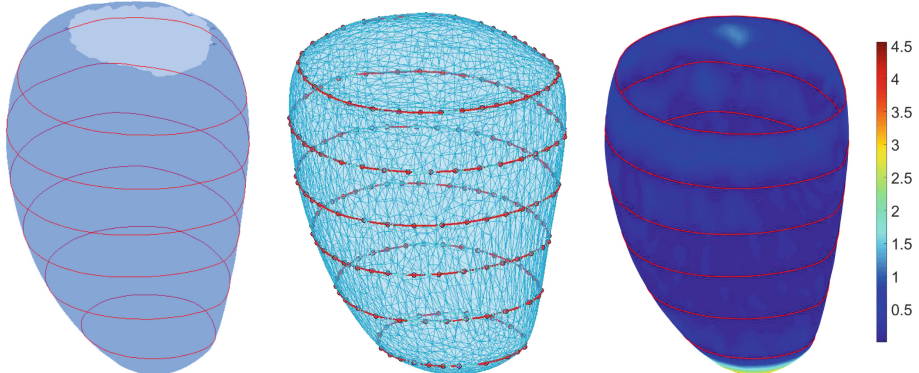


**Fig. 2.** (a) The ground truth mesh (mean shape of a statistical model of the left epicardium) and the synthesized contours in red, (b) our resulting mesh given the red contours, (c) the mesh-to-mesh distance error. the resulting mesh has been clipped at the level of the most basal contour. (Color figure online)

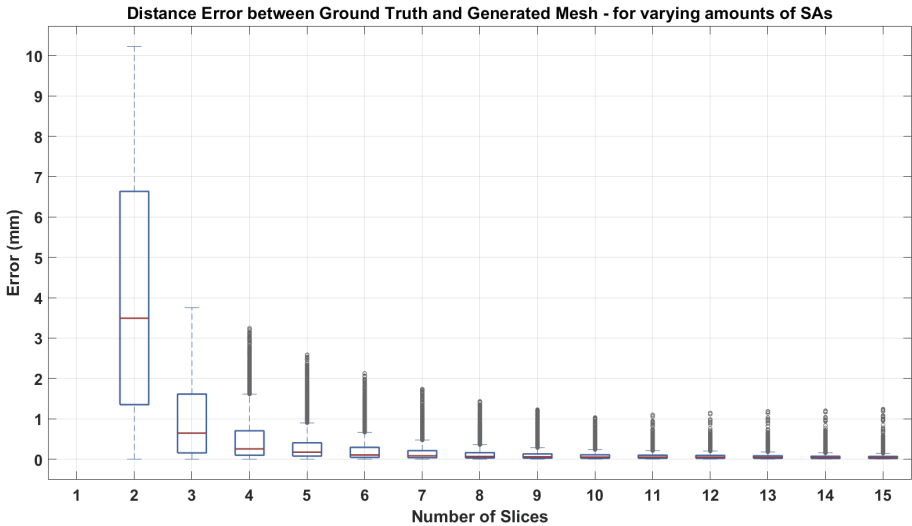


**Fig. 3.** Impact of increasing the amount of SAX has on the error distance between the generated mesh and the ground truth mesh.

**Short Axis and Long Axis Contours.** In a second experiment, we assessed the impact providing LAX contour information had. Similarly to the first experiment, we looked at varying the amount of LAX's and the effect it had on the overall mesh result, as well as look at the influence LAX positions had. Four short axes were chosen as the amount of SAX slices, which was chosen empirically due to the previous experiment, and an increasing amount of long axis contours were provided as the initial input by adding a rotated version of the initial LAX contour every iteration. Likewise, the same analysis was performed, but only keeping two LAX contours every time and only changing their position.

**Non-parallel, Non-coincidental Contours.** As this method is intended to work with clinical data, we simulated a typical set of cardiac contours that is usually obtained. From the mean shape model, 10 SAX contours (resulting in 10 mm inter-slice distance) as well as 2 LAX contours (simulating 2 and 4 chambers view) were generated. This is the equivalent of a typical clinical segmentation set. The contours were then perturbed simulating a breathing misalignment by applying small random translations and rotations (in plane as well as out of plane). The resulting non-parallel, non coincidental contours were given as an input to our algorithm. The resulting mesh can be seen in Fig. 5(a). The distance map overlayed on the mesh is the distance from the resulting mesh to the input contours. The algorithm is also tested on a right ventricle, as seen in Fig. 5(b).

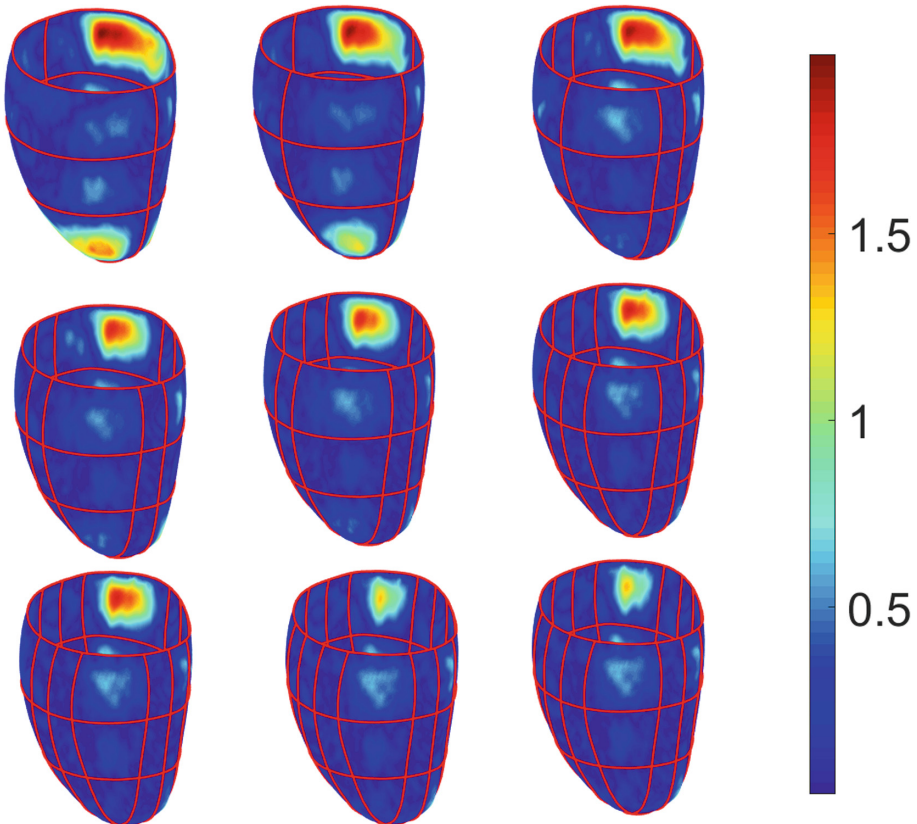


**Fig. 4.** Effect of increasing the amount of LAX contours have on the error distance between the generated mesh and the ground truth mesh.

### 3.2 Clinical Data

Our reconstruction was applied to real clinical data to show how it responds to both normal and pathological cases. As we use the provided expert delineated contours to build the mesh, there is no ground truth to assess our method on. However we performed quantitative analysis on the clinical datasets by measuring the discrepancy between individual contours and the resulting mesh. This measurement provides an evaluation of the “goodness of fit” that the contour has with regards to the mesh. This can be seen in Fig. 8, as the blue box-plots (labelled *OM*). To further evaluate the individual impact each of the contours had on the resulting mesh, we calculated the discrepancy between each of the contours to the mesh, having removed that contour prior to building the mesh. In doing so we assess the ability of our method to interpolate missing information from the dataset. This assessment can be seen in Fig. 8, as the red box-plots (labelled *CM*). It should be noted that the bottom figure contains more boxplots as our HCM dataset contained more contours (13).

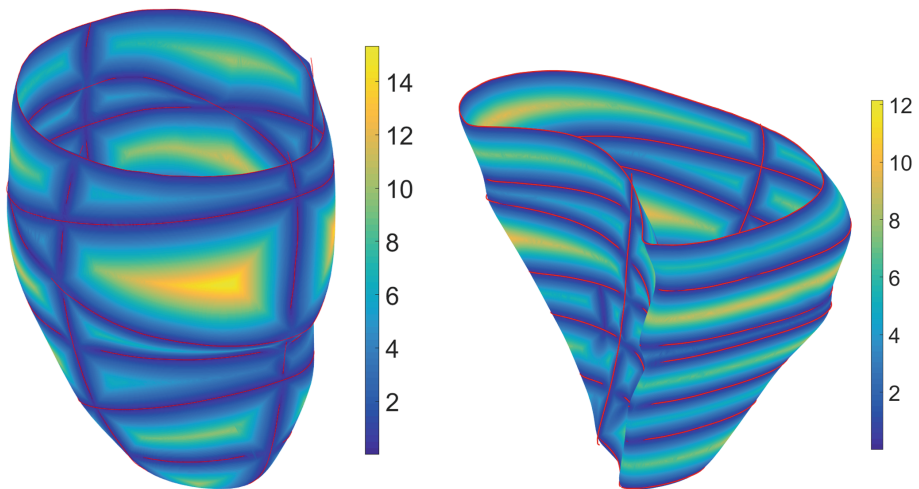


**Fig. 5.** Distance map from the resulting geometrical mesh to the simulated cardiac input data. The contours were transformed by small out of plane rotations and translations.

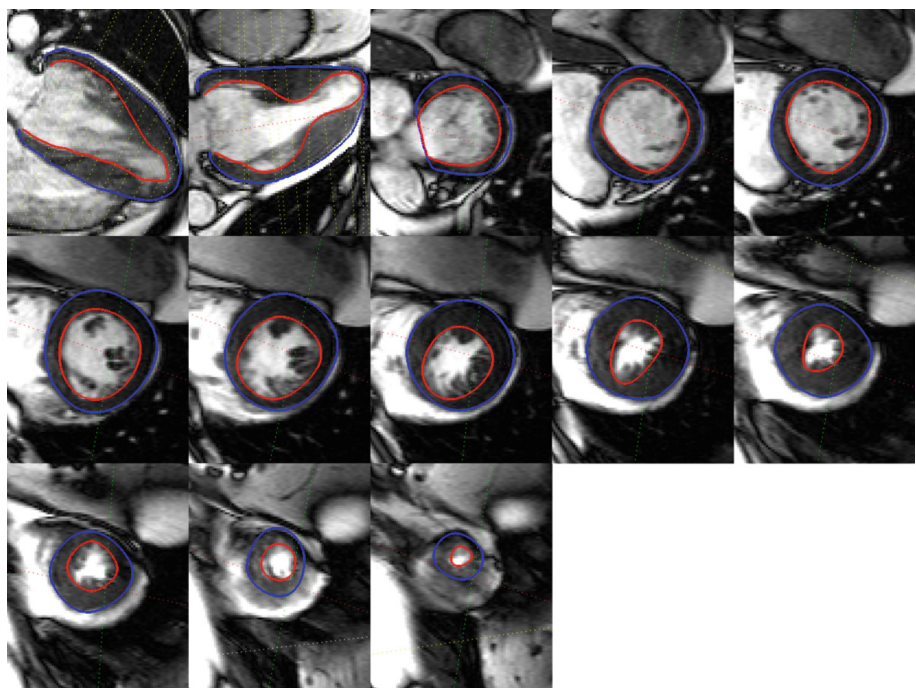


**Fig. 6.** Different clinical contours, delineated by an expert, on a severe case of HCM.

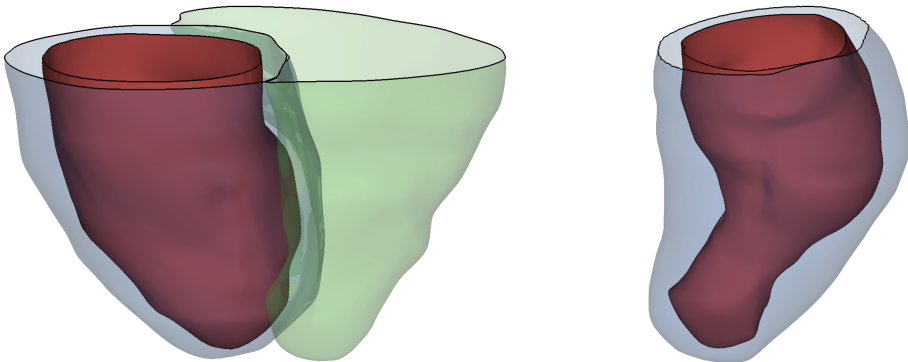


**Fig. 7.** Resulting surface mesh including the left Endocardial and Epicardial ventricle as well as the right Epicardial ventricle obtained from (a) contours for a normal case, and (b) contours belonging to a severe HCM patient.

## 4 Discussion

To be able to assess our process, several experiments were run, ranging from synthetic data using a mean statistical shape model, to severe pathological data. The method was applied to a stack of synthesised parallel contours and the result can be seen in Fig. 2. In order to capture the discrepancy between the ground truth and the resulting mesh, vertex-to-mesh distances were calculated. It can be seen in Fig. 2(c) that the maximum discrepancy error is around 4.5 mm. This error is the distance between the two meshes most apical areas. As we do not have information at the apex due to the absence of LAX, it is expected that this is where the discrepancy would be highest. The other distances however are minimal and appear no greater than 2 mm. To be able to assess the impact the amount of SAX contours have on the process, the distance between meshes was calculated by adding an extra short axis to the input data, in an iterative manner, starting with 2 SAX until a stack of 15. The resulting box plot showing the distances can be seen in Fig. 3. Figure 3 shows that there is a considerable reduction of errors up until 8 slices, after which the decrease in the distance error is not as notable. In this experiment, 8–9 slices represented an average clinical dataset as a SAX stack is generally separated by 10 mm in between. The outliers make up the error distances at the base of the mesh, were no information was provided. The impact that long axes have on the provided data was then assessed. A stack of 4 short axis slices were selected at equidistant positions from base to apex, and two long axes were placed at various different positions. Results showed that the position of the LAX contours had no major contribution to minimising the error distance. We then looked at increasing the number of LAX contours and evaluated the errors, which can be seen in Fig. 4. It can be seen that as the amount of LAX increases, the error decreases, as well as the area with no information. We then looked at generating non parallel, non coincidental contours to simulate clinical data, both with the left and right ventricle. It can

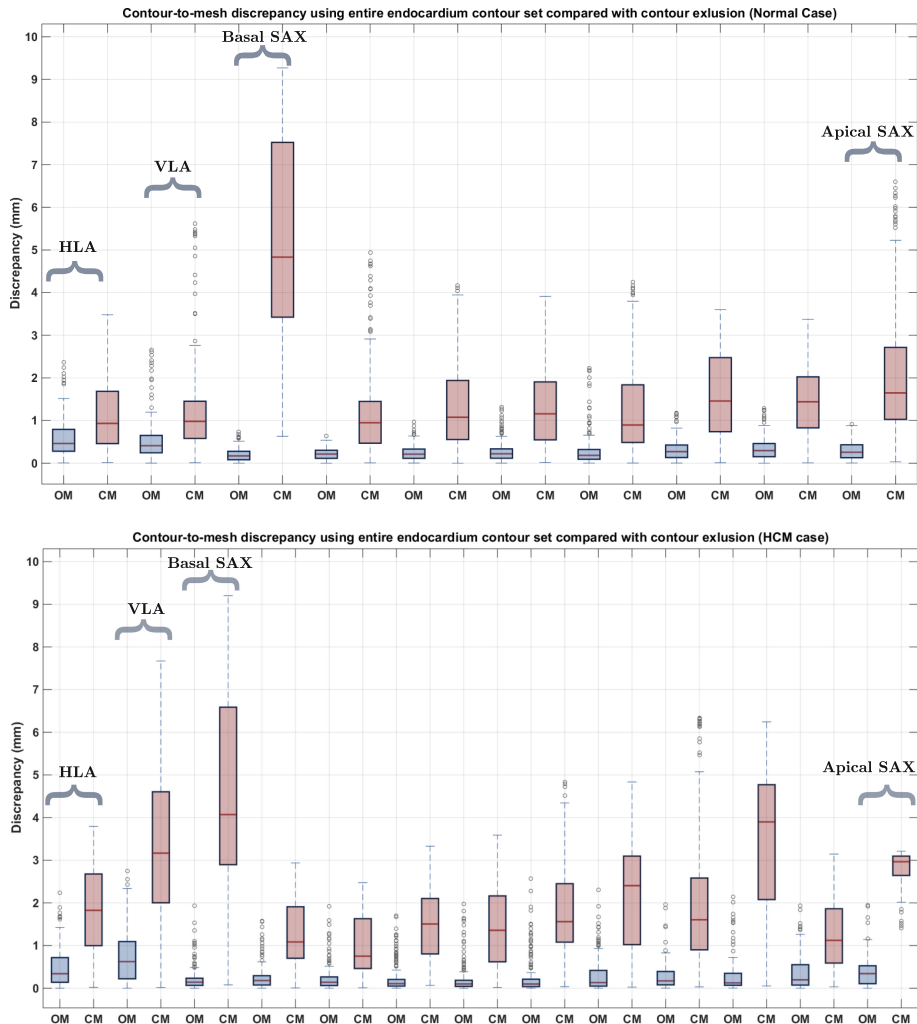


**Fig. 8.** Contour-to-mesh distance having built the mesh with the entire set of contours (labelled *OM*, in blue) and excluded contour-to-mesh distance having built the mesh without the excluded contour (labelled *CM* in red). Top and bottom figures represents the endocardial contours for the normal case, and the HCM case, respectively (Color figure online)

be seen in Fig. 5 that where the contours are, the discrepancy is negligible, and the biggest distance occurs in the areas where there is no information. Despite having non parallel, non coincidental contours, the resulting meshes are visually pleasing. Finally clinical data was used, for both a normal and pathological case. The clinical contours for the pathological case (patient with HCM) can be seen in Fig. 6. The resulting meshes can be observed in Fig. 7. To assess our method's

ability to deal with clinical datasets, we measured the individual contour-to-mesh discrepancies, which can be seen in Fig. 8. It can be seen that when all the contours are used (blue box-plots), the discrepancy is within 1 mm for the normal case (Fig. 7(a)), and 2 mm for the HCM case (Fig. 7(b)). As we proceed to iteratively remove a single contour, in a *leave-one-out* fashion, and rebuild the mesh, the distance for that excluded contour to the mesh increases. It can be seen in both the top and bottom figures, that when the most basal SAX is removed, there is a high discrepancy occurring when measuring the distance from that contour to the resulting mesh. As this is the most basal slice, this is expected as the basal slice contains important structural information about the global geometry of the heart. When the basal slice is removed, our process relies on the LAX to fill in the basal information, which can lead to an early closure of the basal part of the mesh, which might be at a lower geometrical position than the contour, leading to high discrepancy. The removal of contours allows us to assess the individual contributions of the contours to the geometrical result of the mesh. As such, it can be noted that in the case of HCM (Fig. 7(b)), at the positions where the thickening is greatest, when the contours containing valuable information are removed, the discrepancy will be high, which is also the case for the apex. However the discrepancy still falls within 4 mm, except for the basal slice, for the normal case and 7 mm for the HCM case.

## 5 Conclusion

We presented a tool for surface reconstruction applicable to sparse, non parallel, non coincidental, heterogeneous cardiac contours. Our technique works on the left ventricle as well as on the right ventricle. We have empirically shown by means of the exposition of a variety of results, that our technique results in reconstructed interpolating surfaces with very good fitting to the input contours. In the areas to be filled by the interpolated surfaces, our technique presents very pleasant visual appearance. Although the absence of ground truth data precludes fair validations, our technique shows very good agreement against synthetic data.

**Acknowledgments.** BV acknowledges the support of the RCUK Digital Economy Programme grant number EP/G036861/1 (Oxford Centre for Doctoral Training in Healthcare Innovation). VC was supported by ERACoSysMed through a grant to the project SysAFib - Systems medicine for diagnosis and stratification of atrial fibrillation. RA is supported by a British Heart Foundation Clinical Research Training Fellowship. VG is supported by a BBSRC grant (BB/I012117/1), an EPSRC grant (EP/J013250/1) and by BHF New Horizon Grant NH/13/30238. EZ acknowledges the Marie Skłodowska-Curie Individual Fellowship from the H2020 EU Framework Programme for Research and Innovation [Proposal No: 655020-DTI4micro-MSCA-IF-EF-ST].

## References

1. Arevalo, H.J., Vadakkumpadan, F., Guallar, E., Jebb, A., Malamas, P., Wu, K.C., Trayanova, N.A.: Arrhythmia risk stratification of patients after myocardial infarction using personalized heart models. *Nature Commun.* **7** (2016)
2. Zou, M., Holloway, M., Carr, N., Ju, T.: Topology-constrained surface reconstruction from cross-sections. *ACM Trans. Graph. (TOG)* **34**, 128 (2015). Proceedings of ACM SIGGRAPH 2015
3. Sunderland, K., Boyeong, W., Pinter, C., Fichtinger, G.: Reconstruction of surfaces from planar contours through contour interpolations. In: *Image-Guided Procedures, Robotic Interventions, and Modeling, SPIE Proceedings*, vol. 9415 (2015)
4. Deng, D., Zhang, J., Xia, L.: Three-dimensional mesh generation for human heart model. *Life Syst. Model. Intell. Comput. Commun. Inf. Sci.* **98**, 157–162 (2010)
5. Young, A.A., Cowan, B.R., Thrupp, S.F., Hedley, W.J., DellItalia, L.J.: Left ventricular mass and volume: fast calculation with guide-point modelling on MR images. *Radiology* **2(216)**, 597–602 (2000)
6. Lamata, P., Niederer, S., Nordsletten, D., Barber, D.C., Roy, I., Hose, D.R., Smith, N.: An accurate, fast and robust method to generate patient-specific cubic Hermite meshes. *Med. Image Anal.* **15**(6), 801–813 (2011)
7. Albà, X., Pereañez, M., Hoogendoorn, C., Swift, A.J., Wild, J.M., Frangi, A.F., Lekadir, K.: An algorithm for the segmentation of highly abnormal hearts using a generic statistical shape model. *IEEE Trans. Med. Imaging* **35**(3), 845–859 (2016)
8. Lorensen, W.E., Cline, H.E.: Marching cubes: a high resolution 3D surface construction algorithm. In: *ACM SIGGRAPH Computer Graphics*, vol. 21, pp. 163–169. ACM (1987)
9. Villard, B., Zacur, E., Dall'Armellina, E., Grau, V.: Correction of slice misalignment in multi-breath-hold cardiac MRI scans. In: Mansi, T., McLeod, K., Pop, M., Rhode, K., Sermesant, M., Young, A. (eds.) *STACOM 2016. LNCS*, vol. 10124, pp. 30–38. Springer, Cham (2017). doi:[10.1007/978-3-319-52718-5\\_4](https://doi.org/10.1007/978-3-319-52718-5_4)
10. Lopez-Perez, A., Sebastian, R., Ferrero, J.M.: Three-dimensional cardiac computational modelling: methods, features and applications. *Biomed. Eng. Online* **14**, 35 (2015)
11. Zhang, Z., Konno, K., Tokuyama, K.: 3D terrain reconstruction based on contours. In: *9th International Conference on Computer Aided Design and Computer Graphics*, pp. 325–330 (2005)
12. Wang, Z., Geng, N., Zhang, Z.: Surface mesh reconstruction based on contours. In: *International Conference on Computational Intelligence and Software Engineering*, pp. 325–330 (2009)
13. Liu, L., Bajaj, C., Deasy, J.O., Ju, T.: Surface reconstruction from non-parallel curve networks. In: *Eurographics*, vol. 27 (2008)
14. Shi, W., Minas, C., Keenan, N.G., Diamond, T., Durighel, G., Montana, G., Rueckert, D., Cook, S.A., O'Regan, D.P., de Marvao, A., Dawes, T.: Population-based studies of myocardial hypertrophy: high resolution cardiovascular magnetic resonance atlases improve statistical power. *J. Cardiovasc. Magn. Reson.* **16**, 16 (2015)
15. Bai, W., Shi, A.W., Dawes de Marvao, T.J.W., O'Regan, D.P., Cook, S.A., Rueckert, D.: A bi-ventricular cardiac atlas built from 1000+ high resolution MR images of healthy subjects and an analysis of shape and motion. *Med. Image Anal.* **26**(1), 133–145 (2015)

16. Moenning, C., Neil, A.D.: Fast marching farthest point sampling for implicit surfaces and point clouds (2003)
17. Rohr, K., Stiehl, H.S., Sprengel, R., Buzug, T.M., Weese, J., Kuhn, M.H.: Landmark-based elastic registration using approximating thin-plate splines. *IEEE Trans. Med. Imaging* **20**(6), 526–534 (2001)
18. Sprengel, R., Rohr, K., Stiehl, H.S.: Thin-plate spline approximation for image registration. In: Engineering in Medicine and Biology Society, vol. 18 (1996)
19. Garland, M., Heckbert, P.S.: Surface simplification using quadric error metrics. In: Proceedings of 24th Annual Conference on Computer Graphics and Interactive Techniques, pp. 209–216. ACM Press/Addison-Wesley Publishing Co. (1997)